Opportunistic Secondary Communications Downlink Using Multi-Antenna Femtocell Gateways

Brent A. Kenney*, Arslan J. Majid†, Hussein Moradi†, and Behrouz Farhang-Boroujeny*
*Electrical and Computer Engineering Department, University of Utah, Salt Lake City, Utah, USA
†Idaho National Laboratory, Salt Lake City, Utah, USA

***Abstract*—Femtocells can dramatically increase the number of users serviced within a traditional 5G NR cell radius. This paper presents a method for adding femtocells as a secondary network operating in the same spectrum as the primary 5G NR network. The secondary network tailors its transmissions to keep the interference to the primary network to a minimal predefined threshold. Multi-antenna femtocell gateways (FGWs) are introduced, which operate simultaneously as standard user equipments on the primary network and as hubs for the femtocells in the secondary network. Since the downlink of the secondary network must operate through interference from the primary network user equipment (UE) transmissions, a spread spectrum waveform is used along with spectral masking at the femtocell terminals (FTs). Simulation results show that the interference at the base station receiver caused by the secondary FGW transmissions can be kept within a manageable level, allowing hundreds of FGWs to operate harmoniously with the primary network through opportunistic use of the spectrum.**

I. Introduction

Femtocells are widely deployed in cellular networks to increase the level of service where coverage from the cellular carrier is poor. A traditional femtocell is served by an inexpensive, low-power base station (BS) that covers a small geographic area (e.g., 50 m radius), operates using the same spectrum as the cellular carrier, and relies on a wired backhaul to connect to the core network [1]. Because traditional femtocells are consumer-deployed devices and may operate with closed access, interference between the carrier's macrocell and femtocells is a key concern. Although many proposals exist for inter-cell interference mitigation, some proposals side-step the associated complexity of spectral coexistence altogether by specifying a separate portion of the spectrum for femtocells [2]. However, given the scarcity of available spectrum, a shared spectrum approach is highly desirable.

In this paper, we extend the concept of femtocells to a new use case within a 5G NR macrocell. Instead of using femtocells to create pockets of improved coverage for the carrier's network, we propose creating a low-power secondary network that shares the same spectrum as the carrier's primary network and does not impose any new requirements on the primary network for interference mitigation. The proposed femtocells can operate at sufficiently low power by using a spread spectrum waveform and a multi-antenna array at the hub of the femtocell. The hub also can simultaneously communicate on the primary network as standard user equipment (UE). Because the femtocell hub provides connectivity between the primary and secondary networks, it is referred to as the femtocell gateway (FGW). The FGW performs two additional functions in the secondary network. First, as a hub, the FGW facilitates device-to-device (D2D) communication between femtocell terminals (FTs) within a femtocell. Second, the FGW performs data aggregation to package the FTs' uplink data for efficient transmission to the core network. Additionally, FGWs have the advantage of being compatible with vehicle-mounted platforms, if mobility is desired, since the FGW provides a wireless backhaul to the core network. Given the small footprint of the femtocells, several hundred of them could be deployed in a primary network's macrocell (e.g., 1000 m radius) to provide full coverage. A not-to-scale illustration of a few femtocells within a macrocell with the corresponding connections is shown in Fig. 1.

The FTs are low-complexity transceiver devices with low data rate requirements consistent with machine-type communication (MTC). The waveform selected in this study for the secondary network is a special form of spread spectrum called cyclic prefix direct sequence spread spectrum (CP-DSSS). CP-DSSS was first proposed in [3] as a control channel to facilitate ultra-reliable low-latency communications (URLLC). The work in [4] explains the simple transmit and receive structures of CP-DSSS when used as a data channel. The CP-DSSS data frames can be easily synchronized with orthogonal frequency division multiplex (OFDM) frames in the primary 5G NR network (using the 5G NR synchronization signals), leading to several design opportunities for a low-cost, low-power design in a secondary network.

A key innovation that allows the FGW to coexist as a terminal in the primary time-division duplex (TDD) network and a hub in the secondary network is that the secondary network is synchronized to the primary network and operates in the opposite direction. For example, while the primary network BS is receiving uplink (UL) signals, the secondary network FGW transmits downlink (DL) signals to the FTs. Fig. 2 depicts this novel timing allocation.

This manuscript has in part been authored by Battelle Energy Alliance, LLC under Contract No. DE-AC07-05ID14517 with the U.S. Department of Energy. The United States Government retains and the publisher, by accepting the paper for publication, acknowledges that the United States Government retains a nonexclusive, paid-up, irrevocable, world-wide license to publish or reproduce the published form of this manuscript, or allow others to do so, for United States Government purposes. **STI Number: INL/CON-21-62434.**

978-1-6654-2854-5/21/$31.00 ©2021 IEEE

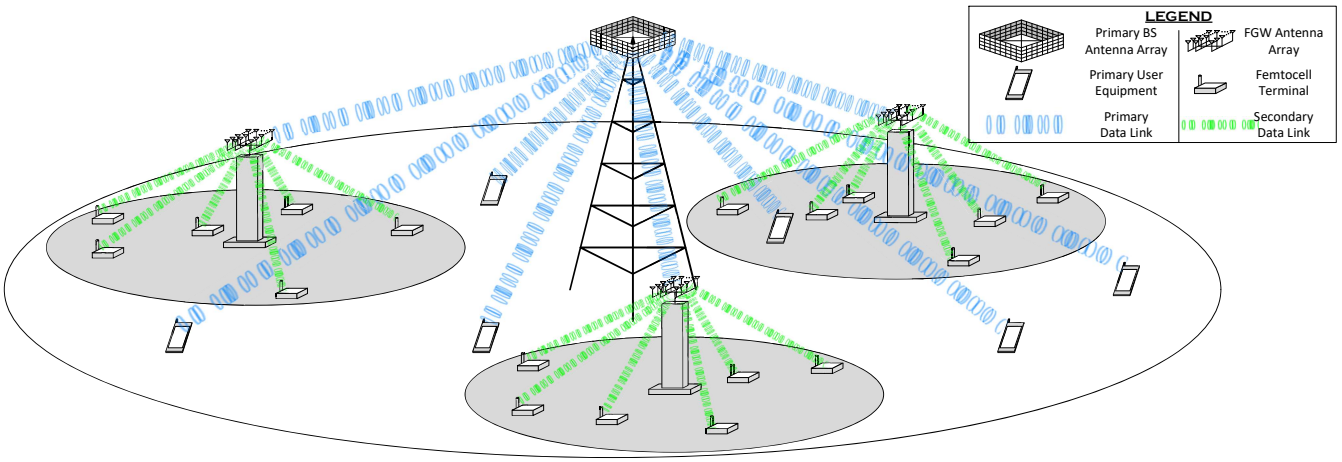

Fig. 1. Illustration of three femtocells (shaded regions) within a 5G NR cell. The BS for the primary network and the FGWs for the secondary network are equipped with multi-antenna arrays. Line-of-sight is not needed for operation. FGWs and FTs may be static or mobile. Not to scale.

Fig. 2. Example of a 1 ms slot allocation for the primary (5G NR) and secondary networks, where the slot is composed of 14 OFDM symbols. This example show 5 UL and 7 DL symbols for the primary network. The secondary network transmits in the opposite direction as the primary network. The secondary network also takes advantage of the guard interval in the primary network to perform channel estimation/training. Training is performed as part of the UL.

Interestingly, primary networks mainly service human-type communication (HTC), which is dominated by DL traffic. Hence, it is likely that the majority of the intervals in a slot will be dedicated to DL traffic. This fact is well aligned with the proposed operation of the secondary network, which transmits in the UL direction during the primary DL intervals. Given that the secondary network services MTC, which is dominated by UL traffic, the secondary network benefits from the primary network's bias toward DL intervals. Several use cases for MTC are presented in [5].

This paper focuses on the DL of the secondary and the UL of the primary networks. In particular, we analyze the interference caused by the UEs of the primary network to the FT receivers, which can be quite significant depending on UE proximity and an FGW's position within the primary network's macrocell. We also examine the interference caused by the FGW transmissions at the BS receiver. We show that through spectral sensing and spectral interference masking, the FT receivers can produce signal-to-interference-plus-noise ratios (SINRs) that result in reliable communications. The details and analysis of the secondary UL and the primary DL transmissions will be covered in a future work.

The remainder of this paper is outlined as follows: Section II provides more details on the interactions between the primary and secondary networks; Section III introduces the system model that governs the frequency domain (FD) processing; Section IV describes how the channel state information (CSI) is estimated for the secondary network; Section V explains how the FT receivers mitigate the effects of the interference from the UE transmissions; Section VI develops an equation for the noise floor impairment at the BS and presents simulation results with a large number of FGWs; Section VII provides concluding remarks.

II. Network Operation

It is assumed that femtocells are located within a 5G NR macrocell. Fig. 1 illustrates a 5G NR BS with a multi-antenna array at the center of the macrocell along with three femtocells in various locations within the macrocell (not to scale). The UEs and the FGWs communicate with the BS as part of the primary network (blue data links). It should be noted that each FGW may have a wired backhaul to the core network, but a wireless backhaul is shown here as an option. The FGW services the FTs within its femtocell as part of the secondary network (green data links). These connections are purposefully narrower than the primary data link, signifying that they are operating at much lower data rates.

Both the primary and secondary networks operate using TDD transmissions. A scheme is devised to limit the amount of interference between the primary and secondary networks, where the secondary network essentially transmits in the opposite direction as the primary network. In this configuration, the FGWs can be present on the primary and secondary networks simultaneously. Fig. 2 shows an example of how the subframes might be allocated for the UL and DL functions for both networks. The processing at the FGW and FTs that allow operation with acceptably low interference to the primary network will be addressed.

In this paper we assume perfect CSI at the BS for all connections between the UEs and the BS. The BS also has perfect CSI for the channels between FGWs and the BS, but the BS assumes that an FGW has a single antenna like any other UE. This information is obtained during the *Training* interval of the primary network indicated in Fig. 2. During this time, the secondary network is essentially silent while it switches from UL to DL. Likewise, we assume that the FGW has perfect CSI for the connections between the FTs and the FGW, but the FGW does not have CSI for its link to the BS. CSI at the FGW is obtained during the *Training* interval of the secondary network, which coincides with the *Guard* interval of the primary network.

III. System Model

We note that the primary network (5G NR) uses OFDM as its modulation format, and we propose CP-DSSS for the secondary network, which is effectively a single carrier modulation (SCM). There are M antennas in the BS array and K layers of spatial multiplexing in the primary network. The FGW has B antennas, and there are D active FTs in each femtocell.

The 1 ms frame defined in Fig. 2 is divided into 14 OFDM symbols or intervals, each with up to N subcarriers in the case of the primary network. For the secondary network, the equivalent spectrum is spanned by N complex samples. Each secondary network transmission will transmit some fraction of N symbols during the OFDM symbol of the primary network, following the CP-DSSS signaling approach.

It is assumed that the length of the channel impulse response (or delay spread) of the primary network, $L_{\text{ch,pri}}$, is less than or equal to the length of the CP plus one. It is reasonable to assume that the delay spread of each femtocell ($L_{\text{ch,sec}}$) is much shorter than $L_{\text{ch,pri}}$, since the delay spread increases with antenna height [6] and the FGW antenna will be mounted lower than the BS antenna in order to service a smaller geographical area. By the same reasoning, 30 kHz and 60 kHz subcarrier spacing numerologies are defined for smaller 5G NR cells in frequency range 1 (sub-6 GHz) [7], where the CP duration is divided by 2 and 4, respectively. The primary network CSI is estimated by sampling the received spectrum, and the secondary network estimates the channel impulse response directly using the method described in Section IV. Although 14 simultaneous users are assumed in this paper per FGW, a shorter channel impulse response in the femtocell means that more than 14 FT channels could be estimated during the *Training* interval (e.g., 56 FTs if the delay spread is compatible with the CP length for 60 kHz subcarrier spacing).

There are four sets of channels that are of concern in this study. All channels are defined by their respective impulse responses in the time domain (TD) or in the FD. Due to the addition of the CP, the TD convolution matrix is circulant in all cases. Consequently, the FD equivalent is a diagonal matrix, where the diagonal elements represent the frequency response of the channel. We will represent all channels in the FD moving forward. The first set of channels defines the propagation between the BS and the F UEs. It is represented as $\mathbf{\Lambda}_{m,f}$. The second set defines the channels between the FGW and the FTs and is represented as $\bar{\mathbf{\Lambda}}_{b,d}$. The third set defines the channels between the BS and the FGW and is represented as $\check{\mathbf{\Lambda}}_{m,b}$. The final set defines the channels between the UEs and the FTs and is represented as $\mathring{\mathbf{\Lambda}}_{f,d}$, although this channel is not being estimated at the current time. Here, the subscript m refers to a BS antenna, f refers to a UE, b refers to an FGW antenna, and d refers to an FT.

We now define the received signals for the primary and secondary network operations. The primary UL signal received at the BS is defined in the FD for each of the M antennas as

$$\tilde{\mathbf{y}}_m^{\text{BS}} = \sum_{f=1}^{F} \mathbf{\Lambda}_{m,f} \tilde{\mathbf{s}}_f^{\text{UL,UE}} + \sum_{b=1}^{B} \check{\mathbf{\Lambda}}_{m,b} \tilde{\mathbf{x}}_b^{\text{FGW}} + \tilde{\mathbf{w}}_m, \tag{1}$$

where the tilde operator denotes a vector in the FD, $\tilde{\mathbf{s}}_f^{\text{UL,UE}}$ is the FD representation of the symbol vector transmitted by the f^{th} UE, $\tilde{\mathbf{x}}_b^{\text{FGW}}$ is the precoded transmission of the FGW for the b^{th} antenna, and $\tilde{\mathbf{w}}_m$ is the receiver noise. Due to resource block (RB) assignments, the majority of the N entries of $\tilde{\mathbf{s}}_f^{\text{UL,UE}}$ will be zero. Note that the precoded signal in the second term contains some interference that affects the received signal at the BS due to the signal components intended for the FTs.

During the primary UL, the FGW is simultaneously transmitting the secondary DL signal. The signal received by the d^{th} FT is defined as

$$\tilde{\mathbf{y}}_d^{\text{FT}} = \sum_{b=1}^{B} \bar{\mathbf{\Lambda}}_{b,d} \tilde{\mathbf{x}}_b^{\text{FGW}} + \sum_{f=1}^{F} \mathring{\mathbf{\Lambda}}_{f,d} \tilde{\mathbf{s}}_f^{\text{UL,UE}} + \tilde{\mathbf{w}}_d, \tag{2}$$

where the first term represents the intended signal, the second term is the interference from the UEs of the primary network, and $\tilde{\mathbf{w}}_d$ is the receiver noise.

IV. Training Intervals

The secondary network opportunistically uses the *Guard* interval before the primary network *Training* interval (see Fig. 2) in order to estimate the channel. Specifically, the FTs transmit a single CP-DSSS symbol at a specific sample delay that is indicated by assignment from the FGW. This transmission is spectrally flat due to the Zadoff-Chu (ZC) sequence used for spreading. When the FGW receiver despreads the received signal, each of the solitary symbols transmitted by the FTs will be convolved by their respective channel impulse response. When each transmitted FT symbol is spaced by $L_{\text{ch,sec}}$ samples or more, there is no overlap between the channel impulse response estimates received by the FGW; see [4] for details.

Since the primary and secondary network training intervals are nearly orthogonal in time, there is little interference between the networks at this stage. We leave the analysis of any interference due to timing offset for a future work. The FGW must use the same precoding during the primary training interval that will be used for normal primary UL

transmissions. The FGW's precoding depends upon the CSI received from the secondary training transmission. Consequently, the secondary *Training* interval is positioned in Fig. 2 to be immediately before the primary training OFDM symbol.

The general approach to the FGW precoding is performed on a frequency bin basis using Zero Forcing (ZF) as defined in [8] for SCM since CP-DSSS is an SCM waveform. During the *Training* interval, the precoded vectors from the FGW in (1) are calculated using an augmented bin-specific channel matrix given as

$$\bar{\mathbf{A}}_n = \begin{bmatrix} \bar{\lambda}_{1,1,n} & \bar{\lambda}_{1,2,n} & \dots & \bar{\lambda}_{1,D,n} & c_1 \\ \bar{\lambda}_{2,1,n} & \bar{\lambda}_{2,2,n} & \dots & \bar{\lambda}_{2,D,n} & c_2 \\ \vdots & \vdots & \ddots & \vdots & \vdots \\ \bar{\lambda}_{B,1,n} & \bar{\lambda}_{B,2,n} & \dots & \bar{\lambda}_{B,D,n} & c_B \end{bmatrix}, \tag{3}$$

where $\bar{\lambda}_{b,d,n}$ is the FD channel corresponding to FGW antenna b, FT d, and frequency bin n (i.e., $\bar{\lambda}_{b,d,n}$ is the n^{th} diagonal element of $\bar{\mathbf{\Lambda}}_{b,d}$). The values c_b are the precoding values for the link between the FGW and the BS. Since the FGW does not have knowledge of the CSI to the BS, the values of the vector $\mathbf{c}$ are left as a design parameter.

The vector of precoded FGW values during the *Training* interval for bin n can be expressed as

$$\tilde{\mathbf{x}}^{\text{FGW,pilot}}_{:,n} = \sqrt{B-(D+1)}\,\bar{\mathbf{A}}^*_n \left(\bar{\mathbf{A}}^{\text{T}}_n \bar{\mathbf{A}}^*_n\right)^{-1} \mathbf{P}^{\frac{1}{2}} \tilde{\mathbf{s}}^{\text{FGW,pilot}}_{:,n}, \tag{4}$$

where $\tilde{\mathbf{x}}^{\text{FGW,pilot}}_{:,n}$ is a vector with B elements, $\mathbf{P}$ is a diagonal matrix representing the transmit power for each FT or BS signal, $\tilde{\mathbf{s}}^{\text{FGW,pilot}}_{:,n}$ is a vector with $D+1$ elements, $(\,)^*$ represents the complex conjugate, and $(\,)^{\text{T}}$ is the transpose. The notation used in (4) closely follows the notation in Section III.A of [9], where a concise derivision is presented. Only the last element of $\tilde{\mathbf{s}}^{\text{FGW,pilot}}_{:,n}$ may be non-zero during the primary training period. Whether or not the last symbol is non-zero depends on the RB assignment given to the FGW from the BS.

The pilot signal received at the BS from the FGW is defined by the bin-specific channel matrix given as

$$\check{\mathbf{A}}_n = \begin{bmatrix} \check{\lambda}_{1,1,n} & \check{\lambda}_{1,2,n} & \dots & \check{\lambda}_{1,B,n} \\ \check{\lambda}_{2,1,n} & \check{\lambda}_{2,2,n} & \dots & \check{\lambda}_{2,B,n} \\ \vdots & \vdots & \ddots & \vdots \\ \check{\lambda}_{M,1,n} & \check{\lambda}_{M,2,n} & \dots & \check{\lambda}_{M,B,n} \end{bmatrix}, \tag{5}$$

where $\check{\lambda}_{m,b,n}$ is the FD channel corresponding to BS antenna m, FGW antenna b, and frequency bin n. Since the primary UEs send pilots that are orthogonal in frequency, we can represent the FGW pilot for the valid bins in a succinct manner. The received pilot signal at the BS is defined as

$$\begin{aligned} \tilde{\mathbf{y}}^{\text{FGW,pilot}}_{:,n} &= \mathbf{P}^{-\frac{1}{2}} \check{\mathbf{A}}_n \tilde{\mathbf{x}}^{\text{FGW,pilot}}_{:,n} \\ &= \sqrt{B-(D+1)}\,\mathbf{P}^{-\frac{1}{2}} \check{\mathbf{A}}_n \bar{\mathbf{A}}^*_n \left(\bar{\mathbf{A}}^{\text{T}}_n \bar{\mathbf{A}}^*_n\right)^{-1} \mathbf{P}^{\frac{1}{2}} \tilde{\mathbf{s}}^{\text{FGW,pilot}}_{:,n}. \end{aligned} \tag{6}$$

Since $\tilde{\mathbf{s}}^{\text{FGW,pilot}}_{:,n}$ is all zeros except for the last element, the observed channel is defined as

$$\lambda^{\text{FGW}}_{:,n} = \check{\mathbf{A}}_n \bar{\mathbf{A}}^*_n \left(\bar{\mathbf{A}}^{\text{T}}_n \bar{\mathbf{A}}^*_n\right)^{-1} [0,\ \dots,\ 0,\ 1]^{\text{T}}. \tag{7}$$

V. Secondary Downlink Interference Avoidance

During the secondary DL intervals, the FGW must precode its transmission to simultaneously transmit OFDM symbols to the BS and a CP-DSSS frame to each of the active FTs. The FGW has CSI for the links to the FTs, but it does not have any CSI to the BS. Hence, the FGW uses the same vector $\mathbf{c}$ used for the primary *Training* interval.

Precoding for the FGW is performed on a frequency bin basis, similar to what is shown in (4). The key difference is that the data sent for each frequency bin contains D elements from the vector $\tilde{\mathbf{x}}^{\text{DL,FT}}_{:,n}$, which is the FD representation of the CP-DSSS signal transmitted to the FTs for bin n. The last element of the transmitted data from the FGW is the primary UL FD symbol, $\tilde{\mathbf{s}}^{\text{UL,FGW}}_n$, which may be zero, depending on RB assignment. The FD precoded vector for bin n is now defined as

$$\tilde{\mathbf{x}}^{\text{FGW}}_{:,n} = \bar{\mathbf{A}}^*_n \left(\bar{\mathbf{A}}^{\text{T}}_n \bar{\mathbf{A}}^*_n\right)^{-1} \left[\left(\tilde{\mathbf{x}}^{\text{DL,FT}}_{:,n}\right)^{\text{T}}, \tilde{\mathbf{s}}^{\text{UL,FGW}}_n \right]^{\text{T}}. \tag{8}$$

The estimated signal for each bin at the FTs is

$$\hat{\tilde{\mathbf{x}}}^{\text{DL,FT}}_{:,n} = \bar{\mathbf{A}}^{\text{T}}_n \tilde{\mathbf{x}}^{\text{FGW}}_{:,n} + \mathring{\mathbf{A}}^{\text{T}}_n \tilde{\mathbf{s}}^{\text{UL,UE}}_{:,n} + \tilde{\mathbf{w}}_{:,n}, \tag{9}$$

where $\mathring{\mathbf{A}}_n$ is the $K \times D$ bin-specific channel matrix between the UEs and the FTs and is formed similarly to (5) using the diagonal elements of the $\mathring{\mathbf{\Lambda}}_{f,d}$ matrices based on RB assignment, and $\tilde{\mathbf{w}}_{:,n}$ is the FT receiver noise. The second term of (9) is the interference from the UE transmissions.

The ZF precoding cancels interfering signals at the intended receiver. Hence, the intended signal is presented at each FT receiver without interference from the other signal components transmitted by the FGW. This is especially important because the FGW's primary UL transmission will be a much higher power than its secondary DL transmissions. Note that interference from adjacent FGWs is not considered in this analysis for two main reasons—the power levels are low compared to the UEs, and ZC sequences with different roots can be used in the CP-DSSS waveform for adjacent cells to further suppress inter-femtocell interference.

Given that the massive MIMO BS uses spatial multiplexing to increase the number of simultaneous users in the band, the macrocell could be servicing many UEs in any given interval. As an example, we assume that each UE is assigned some number of RBs between 2 and 20, and there are 170 RBs in the multiplex with 14 layers of spatial multiplexing. Given a uniform distribution of RBs within the specified limits, the macrocell may have upwards of 200 active UEs in an interval. Since some UEs will be closer to the femtocell than others and each UE only occupies a small portion of the band, the FT receiver has the opportunity to mask out portions of the received spectrum that have high levels of interference.

A. Interference Mitigation through Spectral Masking

As a spread spectrum waveform that spreads each symbol across the entire band, CP-DSSS is well-positioned to cancel strong interference through spectral masking before despreading. This technique consists of three basic steps. First, a threshold is defined to identify RBs with excessive interference. Second, the spectral mask is applied with appropriate shaping to reduce the impulse response length in the TD. Third, the symbols are detected in the TD using the known impulse response from the spectral mask.

The selected threshold determination procedure follows the Forward Cell Averaging method defined in [10]. This method examines all of the spectral power components, sorts them, and then compares each sample to the weighted sum of the previous samples. The coefficient of the weighted sum is statistically determined using the Fisher distribution. In our case, the received spectrum is processed one interval at a time, so there is no spectral averaging for the first interval. However, subsequent intervals could take advantage of averaging.

Secondly, the spectral mask is defined with RB granularity. Although some subcarriers may be above the threshold within an RB, others may not due to frequency selective fading or power variations in high-order modulations. To mitigate this issue, an RB is selected to be masked out if 4 of its 12 subcarriers exceeds the threshold. To shape the spectral mask, we use a raised cosine shape on the adjacent RBs. In order to reduce sharp transitions, a single RB that did not meet the threshold to be masked will still be masked if the neighboring RBs are masked. These precautions help to reduce the impulse response length, which is helpful for detection.

For massive MTC, low-complexity receivers are desirable because they are generally low-power and low-cost. CP-DSSS allows for a low-complexity detection solution by spacing out symbols in the time domain without inducing excessive power variations thanks to the spreading. With the symbols spaced by $L_{\text{CPDSSS}} = 16$ samples, there is sufficient space between symbols to match filter (MF) the despread signal with a truncated version of the impulse response from the spectral masking operation. With this approach, the vast majority of the signal power can be recovered. More complicated means of detecting the signal after spectral masking are available (e.g., decision feedback or minimum mean-squared error equalization), but the MF technique is selected to show a benchmark for performance with a simple detector.

A simulation was conducted with the parameters specified previously to assess the effectiveness of the spectral masking based on the placement of the FGW. A path loss exponent of 3.7 is used. The results are shown in Fig. 3, where the FGW targets a 12 dB signal-to-noise ratio (SNR) prior to UE interference, and 100 random scenarios are simulated at each distance. It is assumed that the UEs use a 64-QAM modulation with a 16 dB target SNR at the BS receiver. The line shows the average achieved SINR versus FGW distance from the BS. At a 100 m distance, there is only a 3 dB drop in SINR from the targeted SNR, but at 700 m, the difference increases to about 9 dB. The difference is larger at farther distances because the UEs in the vicinity of the FTs are transmitting at higher power per subcarrier as they power control to the BS. The rise in SINR beyond 700 m is an artifact of the single macrocell simulation. A multi-cell simulation would show increased degradation beyond 9 dB. The distribution of achieved SINR values follows a Gaussian distribution, and error bars are provided to show the 1σ (approx. 68%) and 2σ (approx. 95%) ranges.

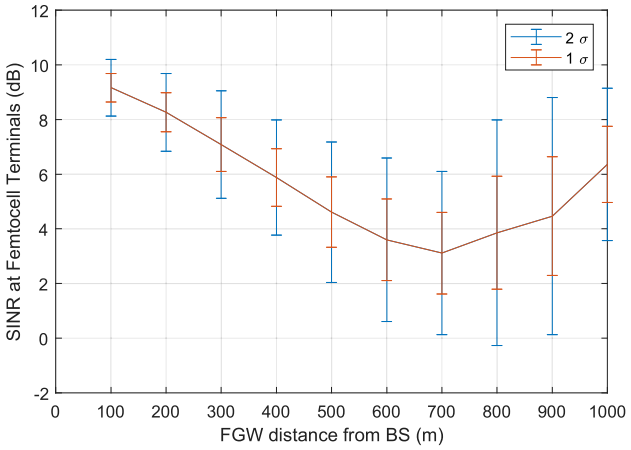

Fig. 3. SINR achieved at the FT due to interference from the UL transmissions of the primary network. The FGW was configured to produce an interference-free SNR of 12 dB at each FT.

The results from Fig. 3 are essential for understanding how transmit power will vary among FGWs depending on their placement in the primary macrocell. If we assume an underlying modulation of QPSK for the CP-DSSS signal with a forward error correction rate of $1/2$, then an SINR target of 3 dB is sufficient at the FT receivers. Additional simulation results confirm that the curve in Fig. 3 responds linearly to the target SNR. As a result, FGWs close to the BS can achieve the target SINR of 3 dB with less power than more distant FGWs. This trend is extremely favorable since nearby FGWs have the most significant impact on the BS receiver.

VI. Interference Analysis for Primary Uplink

The secondary DL transmissions are not cancelled at the BS receive antennas. This extra received power creates interference for the primary UL transmissions from the UEs and the FGWs. The secondary DL power transmitted by the FGW must be kept at a low level since this affects all primary UL signals received at the BS. This section quantifies the interference increase at the BS.

Given that the FGW transmission is optimized to produce a target SNR ($\gamma_{\text{tgt,sec}}$) for FT receiver d, we represent the power per subcarrier as

$$P_d = \frac{\gamma_{\text{tgt,sec}} k_{\text{B}} T_{\text{eq,FT}} W_{\text{sc}}}{G_{\text{Tx}} G_{\text{Rx}} L_d (B - D - 1) L_{\text{CPDSSS}}}, \tag{10}$$

where k_{B} is the Boltzmann constant, $T_{\text{eq,FT}}$ is the equivalent noise temperature of the FT receiver, W_{sc} is the bandwidth

of a subcarrier, G_{Tx} is the transmit antenna gain, G_{Rx} is the receive antenna gain, L_d is the path loss between the FGW and FT receiver d, and L_{CPDSSS} is the data expander factor that spaces the CP-DSSS symbols in the time domain.

The expression for the power of the primary UL signal transmitted from the FGW is governed by the target SNR for the primary receiver ($\gamma_{\mathrm{tgt,pri}}$) and has a similar form given by

$$P_{\mathrm{FGW,pri}} = \frac{\gamma_{\mathrm{tgt,pri}} k_{\mathrm{B}} T_{\mathrm{eq,BS}} W_{\mathrm{sc}}}{G_{\mathrm{Tx}} G_{\mathrm{Rx}} L_{\mathrm{FGW,pri}} (M-\eta)}, \tag{11}$$

where $T_{\mathrm{eq,BS}}$ is the equivalent noise temperature of the BS receiver, $L_{\mathrm{FGW,pri}}$ is the path loss between the FGW and the BS, and η is the number of spacial multiplexed layers used by the BS. Notice that the same antenna gain terms are used for the FT and the BS receivers, but they could be differentiated if desired.

With (10) and (11) defined, we proceed to provide a concise expression for the noise floor impairment, ξ. The noise floor impairment is the ratio of the new noise-plus-interference floor to the old noise floor. For simplicity, we assume that the path losses to all D FTs in the femtocell are equal to the average path loss, $L_{\mathrm{FT,avg}}$. The noise floor impairment caused by one FGW servicing D FTs then reduces to

$$\xi = 1 + \frac{D\ \gamma_{\mathrm{tgt,sec}}\ L_{\mathrm{FGW,pri}}}{(B-D-1)\ L_{\mathrm{CPDSSS}}\ L_{\mathrm{FT,avg}}}. \tag{12}$$

The expression in (12) readily expands to the multi-FGW case by summing the second term over all FGWs in the cell. To create an upper bound on ξ, we simulate a scenario where FGWs are placed in a hexagonal pattern covering the macrocell area. The distance between any two neighboring FGWs is twice the FGW radius or 100 m. In order to show the effect of nearby FGWs versus distant FGWs, we disable FGWs within a stand-off distance from the BS. Hence, fewer FGWs will be active as the stand-off distance increases. Fig. 4 shows two scenarios for the BS noise floor impairment. The blue line shows the impairment with a fixed value of $\gamma_{\mathrm{tgt,sec}} = 12$ dB. The red line uses the results from Fig. 3 to adjust the value of $\gamma_{\mathrm{tgt,sec}}$ of each FGW based on distance from the BS. Notice that with this optimization, all of the FGWs that are spaced as close as 100 m from the BS can be active, and the BS noise floor will be impacted by less than 0.25 dB. Fig. 4 emphasizes the fact that FGWs closest to the BS have the highest impact on the BS noise floor.

VII. Conclusion

This paper presented a framework for a secondary network using the same spectrum as the primary 5G NR network. The secondary network operated opportunisticly without any cooperation from the primary network. The three features that enable low-power operation are multi-antenna FGW terminals, a flexible spread spectrum waveform (CP-DSSS), and spectral masking at the FT receivers to avoid interference from the primary network. We outlined the necessary precoding at the FGW to allow simultaneous operation on the primary and secondary networks. The spectral masking techniques of the

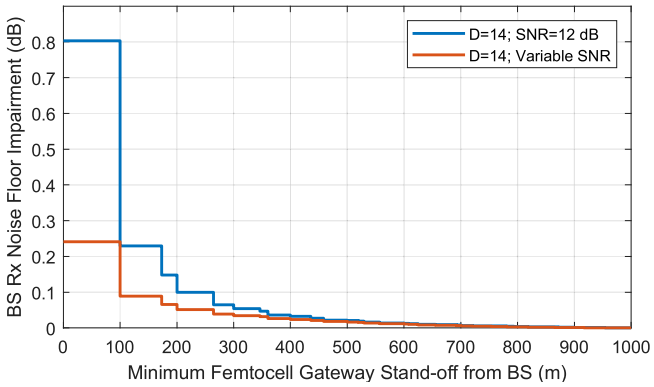

Fig. 4. BS noise floor increase due to multiple FGW transmissions, each communicating with $D = 14$ FTs. The blue line results from a constant pre-interference SNR target, and the red curve represents results where the SNR target is allowed to vary such that the mean SINR at each FT is 3 dB. FGWs are arranged in a hexagonal pattern with a distance of 100 meters to the 6 nearest neighbors. The FGWs cover the entire macrocell, except the central portion specified by the minimum FGW stand-off.

FTs were explained and shown to be effective as a means of opportunistic spectrum reuse. Expressions were provided to estimate the secondary network interference seen by the primary network. Simulation results showed that a primary macrocell could be covered by FGWs with very little effect on the BS receiver noise floor, establishing the viability of this spectrum sharing approach.

References

[1] J. G. Andrews, H. Claussen, M. Dohler, S. Rangan and M. C. Reed, "Femtocells: Past, Present, and Future," *IEEE Journal on Selected Areas in Communications*, vol. 30, no. 3, pp. 497-508, April 2012.

[2] M. Condoluci, M. Dohler, G. Araniti, A. Molinaro and K. Zheng, "Toward 5G densenets: architectural advances for effective machine-type communications over femtocells," *IEEE Communications Magazine*, vol. 53, no. 1, pp. 134-141, January 2015.

[3] A. Aminjavaheri, A. RezazadehReyhani, R. Khalona, H. Moradi and B. Farhang-Boroujeny, "Underlay Control Signaling for Ultra-Reliable Low-Latency IoT Communications," *2018 IEEE International Conference on Communications Workshops (ICC Workshops)*, 2018, pp. 1-6.

[4] B. A. Kenney, S. N. Jenkins, A. J. Majid, H. Moradi and B. Farhang-Boroujeny, "Cyclic Prefix Direct Sequence Spread Spectrum Capacity Analysis," *2020 IEEE 92nd Vehicular Technology Conference (VTC2020-Fall)*, 2020, pp. 1-6.

[5] Z. Dawy, W. Saad, A. Ghosh, J. G. Andrews and E. Yaacoub, "Toward Massive Machine Type Cellular Communications," *IEEE Wireless Communications*, vol. 24, no. 1, pp. 120-128, February 2017.

[6] M. J. Feuerstein, K. L. Blackard, T. S. Rappaport, S. Y. Seidel and H. H. Xia, "Path loss, delay spread, and outage models as functions of antenna height for microcellular system design," *IEEE Transactions on Vehicular Technology*, vol. 43, no. 3, pp. 487-498, Aug. 1994.

[7] E. Dalhman, S. Parkvall, J. Skold, *5G NR: The Next Generation Wireless Access Technology*, London, United Kingdom: Academic Press, 2018.

[8] Z. Mokhtari, M. Sabbaghian and R. Dinis, "Massive MIMO Downlink Based on Single Carrier Frequency Domain Processing," *IEEE Transactions on Communications*, vol. 66, no. 3, pp. 1164-1175, Mar. 2018.

[9] B. A. Kenney, A. J. Majid, H. Moradi and B. Farhang-Boroujeny, "Efficient Precoding for Single Carrier Modulation in Multi-User Massive MIMO Networks," *ICC 2021 - IEEE International Conference on Communications*, 2021, pp. 1-6.

[10] J. J. Lehtomaki, J. Vartiainen, M. Juntti and H. Saarnisaari, "Spectrum Sensing with Forward Methods," *MILCOM 2006 - 2006 IEEE Military Communications conference*, 2006, pp. 1-7.